Corresponding Author:
Don Chambers
chambers@csr.utexas.edu

Global Mean Sea Level Change and the Earth's Water Mass Budget

Don P. Chambers, Jianli Chen, R. Steven Nerem, and Byron D. Tapley
Center for Space Research, The University of Texas at Austin

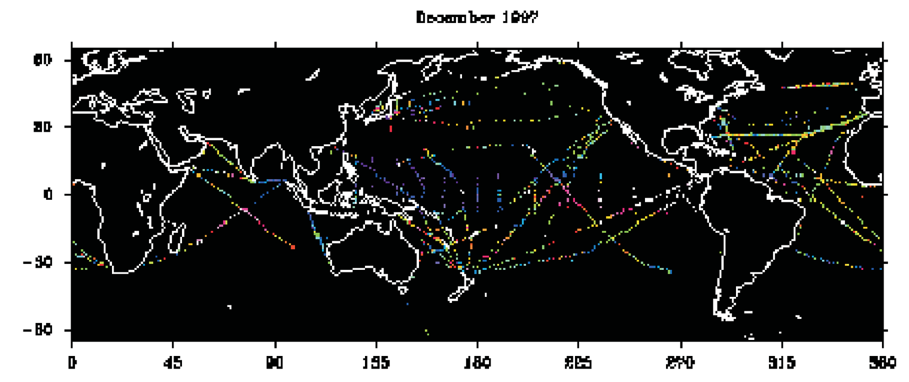

Figure 1. **Raw** XBT data for December 1997.

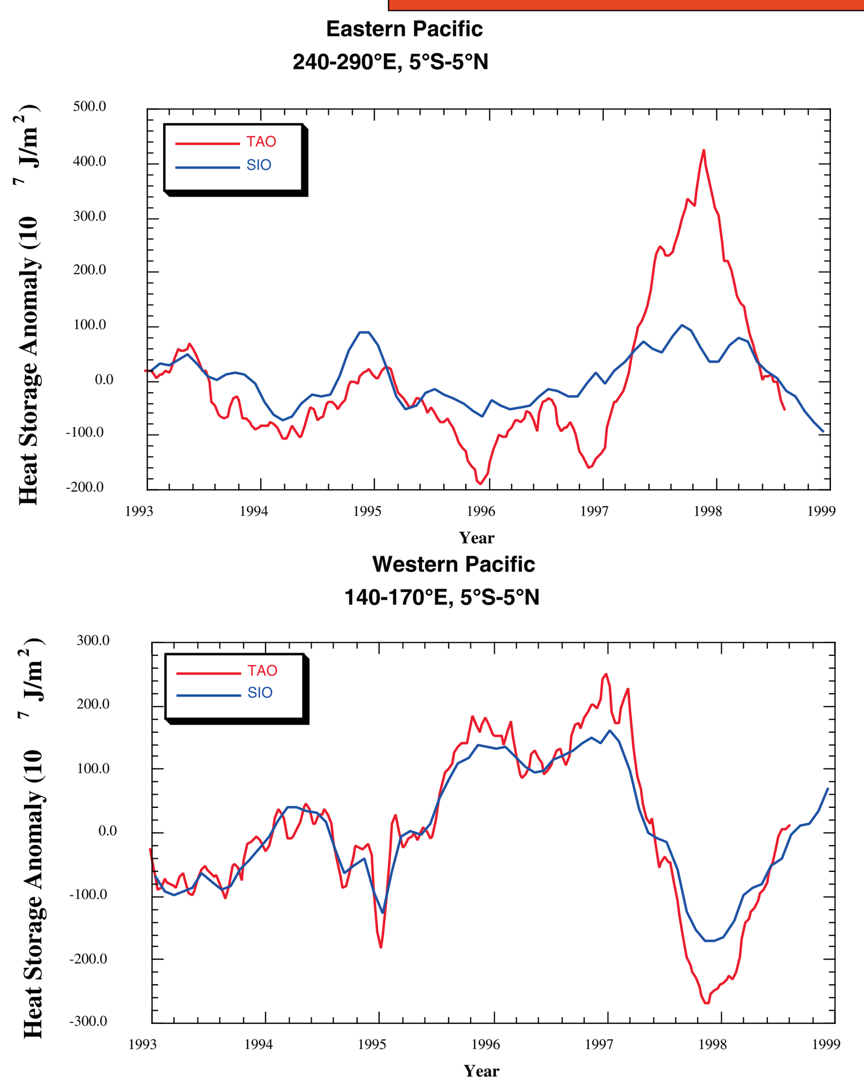

Figure 2. Heat storage anomalies (i.e., thermal sea level) in equatorial Pacific from TAO buoys (red curve) and SIO interpolation of XBT data (blue curve).

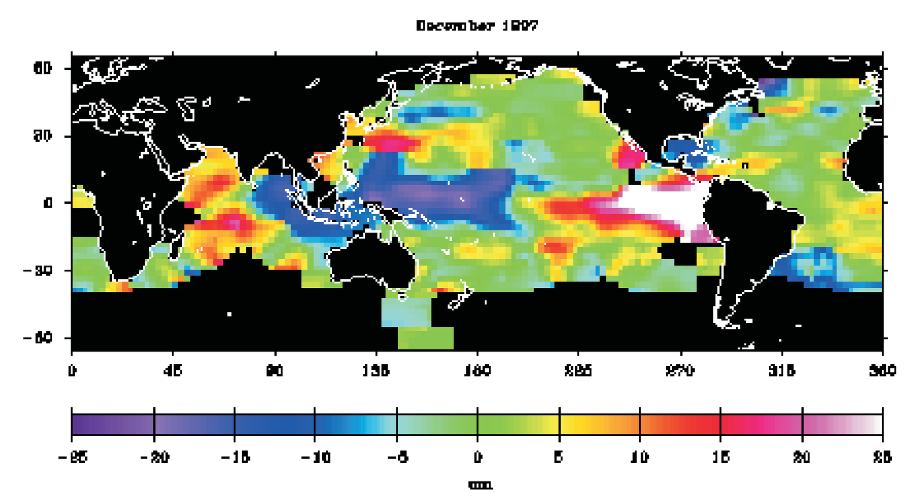

Figure 3. XBT data for December 1997 after interpolating with a long-wavelength filter identical to that used with T/P data.

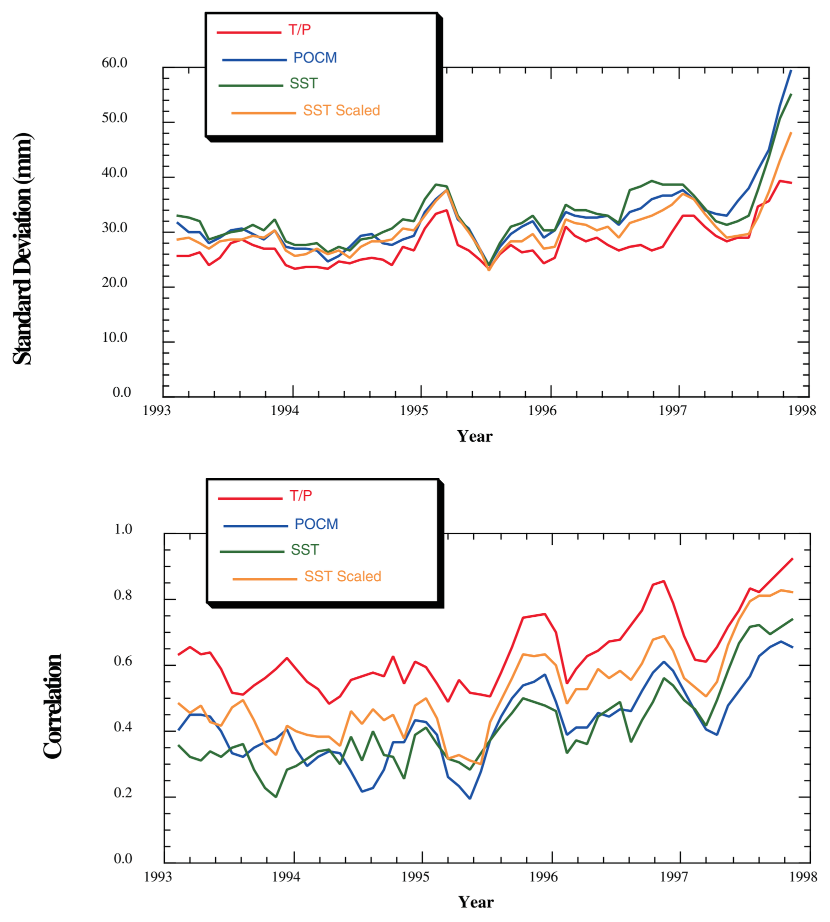

Figure 4. Comparison of EOF reconstruction with various sources of EOF modes, compared to a long-wavelength filtered set of XBT data. The T/P EOFs were selected as a basis function based on the smallest standard deviation and highest correlation.

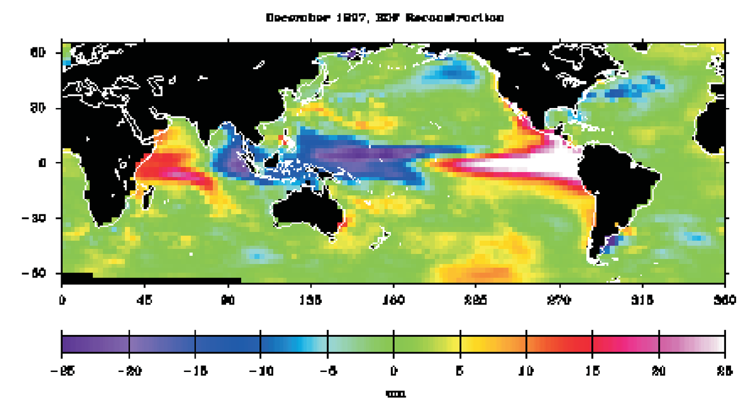

Figure 5. XBT data for December 1997 after interpolating with EOF reconstruction.

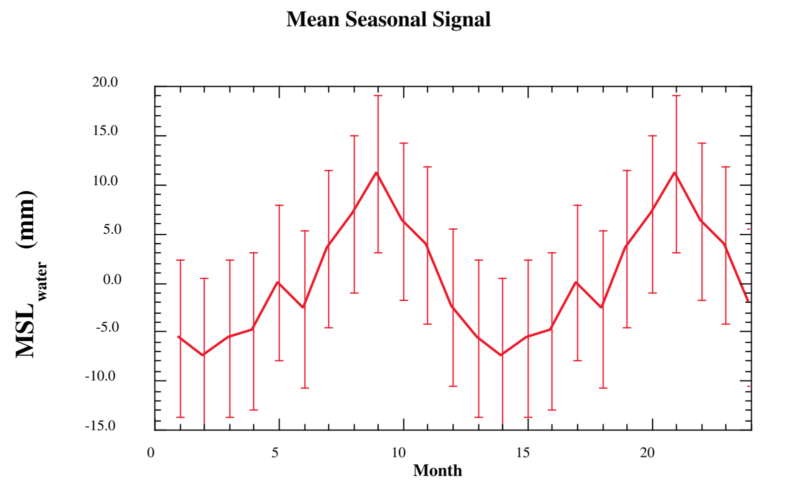

Figure 6. Seasonal signal of ΔMSL_{water} determined from Equation (6). The monthly values have been averaged for years 1993 to 1998. Two complete cycles are shown. The error bars are 1-σ from Table 1.

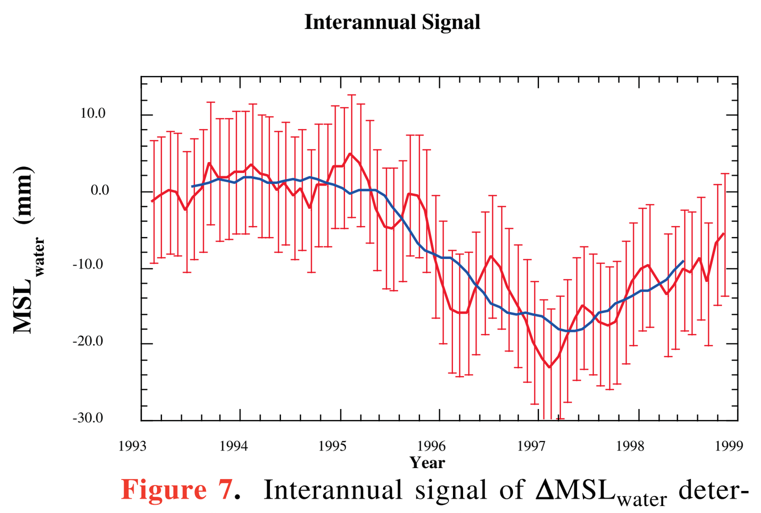

Figure 7. Interannual signal of ΔMSL_{water} determined from Equation (6) after removing mean seasonal signal shown in Figure 6. The smooth blue curve is the 365-day boxcar filtered time-series. The error bars are 1-σ from Table 1.

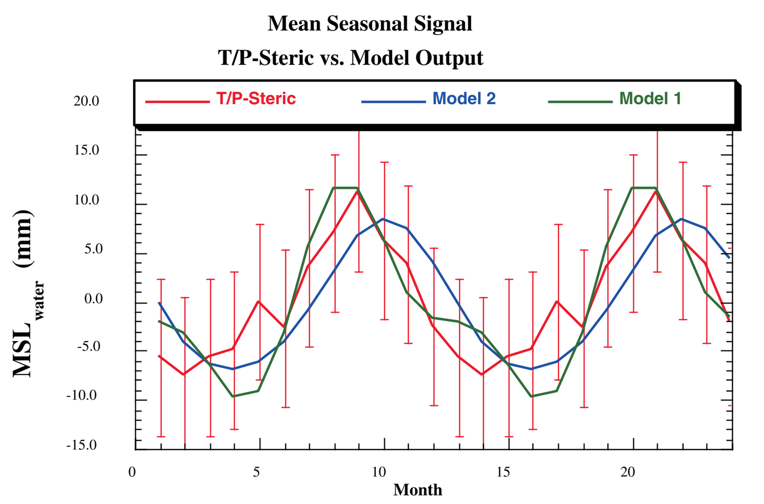

Figure 8. Seasonal signal of ΔMSL_{water} for T/P-Steric and output from two models.

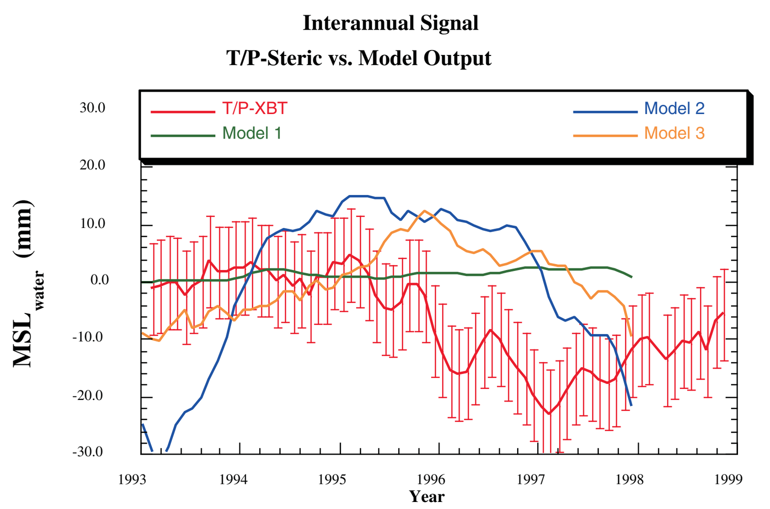

Figure 9. Interannual signal of ΔMSL_{water} for T/P-Steric and output from three models.

Table 1. Summary of errors estimated for ΔMSL_{water}.

Error Source	Annual σ (mm)	Interannual σ (mm)
XBT Error	3	2
XBT Sampling after 1996	1	4
XBT Sampling of GMSL	6	3
T/P Error	3	3
Salinity Signal	1	3
Gridding Error	3	3
IB error and barotropic signal	2	2
RSS	8	8

Table 2. Annual and semiannual variations in ΔMSL_{water} determined from T/P and models.

	Annual		Semiannual	
Source	amp	phase	amp	phase
T/P-XBT	7.6 ± 1.3	266 ± 10	2.1 ± 1.3	108 ± 19
Model 1	8.9	278	4.2	338
Model 2	7.7	307	0.7	133
Model 3	26.8	301	2.3	90

amp is in mm
phase is in days past Jan. 1, 1993, 0h:0m UTC

Introduction

Global mean sea level changes measured directly by satellite altimetry [e.g., *Nerem*, 1995] are directly related to changes in the volume of the oceans due to fresh water and heat fluxes. The relative contribution of water mass exchange and heat change cannot be determined from altimetry alone, however. To study the fresh water mass variations, the portion of the signal related to the steric effects must be removed. Steric effects are those density variation which result in a volume change but no mass change, such as thermal and salinity expansion and contraction.

Generally, the salinity signal is ignored, because to first order the steric signal is dominated by thermal variations [*Gill and Niiler*, 1973]. Previously, we have examined the global ocean water mass variations at an annual period by removing a steric model based on climatology [*Chen et al.*, 1998]. However, for interannual periods, signals such as El Niño will be misinterpreted as mass variations if a climatology is used, as these variations are mainly thermal [*Chambers et al.*, 1998a].

To study both annual and interannual thermal and mass signals in global mean sea level change during the TOPEX/Poseidon (T/P) mission, we have examined data from expendable bathythermographs (XBTs) that are released by ships of opportunity. Thus they are most dense along shipping routes, leaving much of the ocean undersampled (**Figure 1**). To use the XBT data for global studies, they must be interpolated to a uniform grid, such as the grids computed by *White* [1995] at the Scripps Institute of Oceanography (SIO). However, this method grids data only north of about 30°S. Also, recent analysis indicates that the method tends to underestimate the amplitude of heat storage by a factor of as much as two to three in the tropics and southern hemisphere [*White et al.*, 1999]. This is demonstrated in **Figure 2**, where the SIO grids severely underestimate the El Niño signal in the eastern and western equatorial Pacific.

Data Processing

T/P altimeter data come from the MGDR-B release for Cycles 10-231. Sea level anomalies are computed and averaged over months from January, 1993 to December, 1998, then gridded into 2.5° grids and smoothed with a long wavelength filter [*Chambers et al.*, 1997]. An inverted barometer correction which takes into account the time-varying mean pressure over the ocean is applied [*Raofi*, 1997]. Data are corrected for the TMR drift [Zlotnicki, personal communication, 1999].

The XBT data are from the National Oceanographic Data Center [*Hamilton*, 1994]. All profiles have been statistically and visually compared to temperature profiles from the World Ocean Atlas 1994 (WOA94) database [*Levitus and Boyer*, 1994], and spurious profiles have been removed. All profiles with a maximum depth less than 300 m were also edited. The sea level anomaly (Δη) for the XBT data was computed relative to WOA94 mean temperatures

$$\Delta\eta = \int_{-h_{max}}^{0} \alpha(z,T,S)\left(T_{XBT}(z) - T_{WOA}(z)\right)dz \qquad (1)$$

where α is the thermal expansion coefficient computed from an equation of state [*Gill*, 1982]. The XBT sea level anomalies are then gridded to a 2.5° grid similar to T/P, but not smoothed.

The EOF reconstruction technique [*Smith et al.*, 1996] uses the spatial maps from a principal component analysis as multiple covariance basis functions in place of a single covariance function as in optimal interpolation. If the gridded basis data are defined as $O(x,t)$, then

$$O(x,t) = \sum_{k=1}^{N} T_k(t)X_k(x) \qquad (2)$$

where x is the two-dimensional space domain, t is time, k is the EOF mode, N is the maximum number of modes, $T_k(t)$ is the time series for each mode, and $X_k(x)$ is the spatial map for each EOF mode. For the reconstruction process, the gridded XBT sea level anomaly data are defined as $I(x,\tau)$, where T is the discrete monthly time index.

We set up a linear relationship between the XBT data and the EOF modes as

$$\varepsilon = I(x,\tau) - \left[a + \sum_{k=1}^{N} W_k(\tau)X_k(x)\right], \qquad (3)$$

where a is an unknown bias, $X_k(x)$ are the EOF spatial modes from (2), and $W_k(\tau)$ are the unknown temporal modes. We solve for the unknowns (a, $W_k(\tau)$) via a least-squares procedure to minimize ε.

The final step is to compute the reconstructed anomaly $R(x,\tau)$ by using the estimated parameters (designated by <>)

$$R(x,\tau) = \langle a\rangle + \sum_{k=1}^{N} \langle W_k(\tau)\rangle X_k(x). \qquad (4)$$

Since global maps of interannual thermal sea level variability are not available, we have examined several proxy data to use for EOF maps. These include the same global SST data used by *Smith et al.* [1996], heat storage anomalies to 400 m computed from the Parallel Ocean Climate Model (POCM) [*Stammer et al.*, 1996], and total sea level anomaly data from T/P. Tests indicate that the results using the T/P EOFs give the best results (**Figure 4**), so these are used for the EOF reconstruction. **Figure 5** shows the map for the same data shown in **Figure 1** after the EOF reconstruction.

Results and Error Analysis

The global mean sea level change (ΔMSL) is computed from each monthly grid as

$$\Delta MSL = \frac{\sum_{65°S}^{65°N} \Delta\eta \cdot da}{\sum_{65°S}^{65°N} da}, \quad da = \cos(latitude) \qquad (5)$$

The mean sea level change due to fresh water mass (ΔMSL_{water}) is computed from

$$\Delta MSL_{water} = \Delta MSL_{T/P} - \Delta MSL_{XBT} + \varepsilon \qquad (6)$$

where ε represents errors in the data as well as errors in neglecting steric effects due to salinity changes.

We have further reduced ΔMSL_{water} into a mean annual component and an interannual component. The annual component was computed by averaging all data for each month (**Figure 6**). The interannual component was computed by removing the mean monthly values and smoothing with a running mean boxcar filter over 3 months (**Figure 7**).

The errors, ε, arises from the following sources, which are summarized in **Table 1**:

1) XBT error and interpolation error: standard deviation (σ) between reconstructed grids and long-wavelength filtered grids. The long-wavelength filter is completely independent of the EOF reconstruction.

2) XBT sampling error because of lower number of observations after 1996: redid reconstruction with data reduced to areas with an observation in November, 1997 (minimum); σ between original and sampled reconstruction.

3) Sampling error of fewer XBT data compared to T/P: sampled T/P to XBT raw grids; σ between GMSL from T/P full and T/P sampled.

4) T/P error: σ of average difference between T/P and island tide gauges.

5) Salinity signal: for annual, based on comparing WOA94 data using monthly and mean salinity values. Since there is no good estimate for interannual signals, we scaled the annual magnitude up by 2.5 based on average ratio of other errors.

6) Gridding error: the gridded GMSL for T/P differs slightly from the value computed from the 1-sec data. Error in gridding estimated as σ of difference between gridded and 1-sec time-series.

7) IB error and barotropic signal: IB error from *Raofi* [1998]; barotropic signal from standard deviation of GMSL computed from barotropic model [*Ponte*, 1999] between 65°S and 65°N.

Discussion

ΔMSL_{water} can also be computed from outputs from atmospheric general circulation models (AGCM) [*Chen et al.*, 1998]:

- **Model 1**: continental soil moisture/snow + precipitable water in atmosphere from NCEP reanalysis . Since water mass is conserved,

$$\Delta M_{ocean} + \Delta M_{land} + \Delta M_{atmos} = 0,$$
$$\Delta M_{ocean} = -(\Delta M_{land} + \Delta M_{atmos}). \qquad (7)$$

  The equivalent mean sea level change is:

$$\Delta MSL_{water} = (\Delta M_{ocean}/\rho_0 A_{ocean}), \qquad (8)$$

  where is the ρ_0 density of fresh water and A_{ocean} is the area of the ocean.

- **Model 2**: ocean precipitation (P), evaporation (E), and runoff (R) from NCEP.

$$\frac{dS(t)}{dt} = \iint_{ocean} (P - E + R)dxdy, \quad P - E + R \ \text{unbiased}$$

$$\Delta M_{ocean}(t) = \rho_{water}\int_0^t \frac{dS(\tau)}{d\tau}d\tau \qquad (9)$$

- **Model 3**: similar to Model 2, except using land precipitation and potential evaporation, and computing (P-E-R). Then, add precipitable water and compute equivalent ocean variation from (7).

The seasonal signal from T/P-XBT agrees with the output from the models within 1-σ for Models 1 and 2 (**Figure 8, Table 2**). Model 3 has too large of an annual amplitude, most likely from using potential evaporation, which assumes unlimited ground water. The phases of all the models agree with T/P-XBT within 2-σ, except for the semiannual phase of Model 2, which differs from T/P-XBT by 135 days. The amplitude for the semiannual component of Model 2 is also the largest of all the models or T/P-XBT. These results are similar to the those presented by *Chen et al*. [1998].

The interannual signal has never been discussed and is as large as the seasonal cycle (**Figure 7**). Is this variation also due to fresh water storage as the seasonal cycle appears to be, or is due to another factor? Although the number of XBT profiles did decrease in 1996-1997, we tested whether this could be responsible in two ways (Cases 2 and 3 in the error analysis). Neither test indicated the sampling could cause an error this large. Another source which has been suggested in previous presentations is that the lower levels (below XBT data) cooled at the same time as the surface layers warmed. The warming surface layers can be explained by circulation changes associated with the 1997 El Nino, which reduced the Ekman drift away from the equator in the tropical Pacific. This led to water staying longer in the tropics to be warmed by the sun, as well as a decrease in upwelling of cool water from below the thermocline.

However, we can find no mechanism to explain a cooling deep layer. The cold waters below the thermocline cannot loose heat to the warm, upper layer. Nor is it likely that the heat was lost to the solid earth. An approximate calculation indicates that the solid earth at the boundaries would have had to cool by more than 10°C in a matter of months to explain the signal seen in **Figure 7**.

Furthermore, although the models disagree among themselves (**Figure 9**), two do show interannual variations with similar magnitudes, although different frequencies and phases. Models 2 and 3 show a general decrease in MSL attributable to loss of water from the ocean during 1997, although it is nearly a year out of phase with the T/P-XBT results. These results emphasize the problems current models have in determining the interannual hydrological cycle.

Conclusions

Our results agree well with models and other observations for the seasonal cycle of water mass storage in the ocean. For interannual variability, the results of this study suggest that the ocean lost about 15 mm more water than normal per square meter between 1995 and 1997. The error analysis indicates the value is significant at the 95% confidence level. This is about the same amount of water lost from peak storage to minimal storage during the seasonal cycle. Thus, from 1995 to 1997, the seasonal cycle was nearly doubled.

Although the models do not agree well with the observations for the interannual variation, two of them do predict a similar magnitude of change, which suggests that the change observed by T/P and the XBT data is reasonable. A complete verification of the interannual T/P-XBT observations is impossible, however, because there simply are no other similar observations except model output. In the near future, we hope to examine lake level change over the same time period, and see if it matches the indicated oceanic water mass lost. Although not all of the water lost will end up in lakes, and portions of the lake level rise will be attributable to changing ground water storage, we expect that there should be a correlated signal in the global mean lake level variations.

The best validation of this technique will not be possible for several years, however. By then, the Gravity and Climate Experiment (GRACE) should be monitoring changes in the gravity field associated with water mass variations in the Earth system components. By comparing the Jason-XBT results with GRACE data over the same time period, we should be able to put a better error bar on the Jason-XBT interannual and seasonal observations of water mass storage in the ocean. If the Jason-XBT results have reasonable accuracy, we can use the T/P-XBT results to produce a decadal time-series of mean water mass storage in the Earth's oceans.

References

Chambers, D. P., B. D. Tapley, and R. H. Stewart, Long-period ocean heat storage rates and basin-scale heat fluxes from TOPEX, *J. Geophys. Res., 102* (C5), 10525-10533, 1997.
Chambers, D. P., B. D. Tapley, and R. H. Stewart, Measuring heat-storage changes in the equatorial Pacific: a comparison between TOPEX altimetry and TAO buoys, *J. Geophys. Res., 103* (C9), 18591-18597, 1998a.
Chen, J. L., C. R. Wilson, D. P. Chambers, R. S. Nerem, and B. D. Tapley, Seasonal global water mass balance and mean sea level variations, *Geophys. Res. Ltrs*., 25, 3555-3558, 1998.
Gill, A. E., *Atmosphere-Ocean Dynamics*, 662 pp., Academic, San Diego, CA, 1982.
Gill, A. E., and P. P. Niiler, The theory of the seasonal variability in the ocean, *Deep-Sea Res*., 20, 141-177, 1973.
Hamilton, D., GTSPP builds an ocean temperature-salinity database, *Earth System Monitor*, June, 1994.
Levitus, S., and T. P. Boyer, *World Ocean Atlas 1994,* vol. 2, *Temperature*, *NOAA Atlas NESDIS 2*, 99 pp., Natl. Oceanic and Atmos. Admin., Silver Spring, Md., 1994.
Nerem, R. S., Measuring global mean sea level variations using TOPEX/POSEIDON altimeter data, *J. Geophys. Res.*, *100*, 25135-25151, 1995.
Raofi, B., Ocean's response to atmospheric pressure loading: The inverted barometer approximation for altimetry measurements, *CSR-98-1*, Center for Space Research, Austin, TX, 1998.
Smith T. M., R. W. Reynolds, R. E. Livezey, and D. C. Stokes, Reconstruction of historical sea surface temperatures using empirical orthogonal functions, *J. Climate, 9*, 1403-1420, 1996.
Stammer, D., R. Tokmakian, A. Semtner, and C. Wunsch, How well does a 1/4° global circulation model simulate large-scale oceanic observations?, *J. Geophys. Res., 101*, 25,779-25,812, 1996.
White, W. B., Design of a global observing system for basn-scale upper ocean temperature changes, *Prog. Oceanogr.*, *36*, 169-217, 1994.
White, W. B., D. Cayan, and J. Lean, Global upper ocean heat storage response to radiative forcing from changing solar irradiance and increasing green-house gas/aerosol concentrations, *J. Geophys. Res., 103* (C10), 21,355-21,366, 1998.

Acknowledgments. This research was supported by NASA grant NAG5-6309.